SC-Triggered 1.6mHz Waves Including an Interval with Latitude-Dependent Phase Shift, Observed by the SuperDARN Hokkaido East Radar in Mid Latitudes: Possible Global Magnetospheric Cavity-Mode Waves and Their Field-Line Resonance with Poloidal Alfven-Mode Waves

Kawano, Hideaki
Department of Earth and Planetary Sciences, Faculty of Sciences, Kyushu University : Associate Professor

Yukimatsu, Akira Sessai
National Institute of Polar Research

Tanaka, Yoshimasa
National Institute of Polar Research

Satoko, Saita
Department of Electronics & Control Engineering, Kitakyushu National College of Technology

他

https://doi.org/10.5109/1785877

出版情報：九州大学大学院理学研究院紀要 : Series D, Earth and planetary sciences. 34 (1), pp.1-15, 2016-11-21. Faculty of Science, Kyushu University
バージョン：
権利関係：

Mem. Fac. Sci., Kyushu Univ., Ser. D, Earth & Planet. Sci., Vol. XXXIV, No. 1,
pp. 1-15, November 00, 2016

SC-Triggered 1.6mHz Waves Including an Interval with Latitude-Dependent Phase Shift, Observed by the SuperDARN Hokkaido East Radar in Mid Latitudes: Possible Global Magnetospheric Cavity-Mode Waves and Their Field-Line Resonance with Poloidal Alfven-Mode Waves

Hideaki Kawano*, Akira Sessai Yukimatu**, Yoshimasa Tanaka**, Satoko Saita***,
Nozomu Nishitani****, and Tomoaki Hori****,*****

Abstract

In this paper we present a new kind of wave event found in the ground/sea backscattered data of the SuperDARN Hokkaido East radar, located in the mid-latitude area at the AACGM latitude (longitude) of 36.5° (214.7°). The wave event started at the time of an SC at ~09:50 UT on Aug 19, 2009, and continued for about an hour until ~10:50 UT: This relatively short-living wave event, probably triggered by the SC, could be classified as a type different from the typical type seen in the ground/sea backscattered data of SuperDARN radars, i.e., waves which start without a clearly identifiable trigger and continue for a long time (4~5 hours) (e.g., Ponomarenko et al. 2003). Comparisons with ground magnetometer data suggest that the major part of this event consisted of global magnetospheric cavity-mode waves whose typical frequency is in the order of 1mHz (e.g., Kivelson and Southwood 1985, 1986). In addition, in the interval of 10:26~10:42UT which was embedded in the above-stated one-hour interval, we have found the amplitude and phase pattern typically observed when the field-line resonance (FLR) takes place; this pattern is found for the first time in the mid-latitude ground/sea backscattered data, and suggests excitation of poloidal Alfven-mode field-line eigenoscillations during this interval.

Keywords: SuperDARN Hokkaido East radar, mid-latitude observation, SC-triggered waves, global magnetospheric cavity-mode waves, field-line resonance (FLR)

1. Introduction

SuperDARN stands for Super Dual Auroral Radar Network (Greenwald et al. 1995). It is a global network of HF radars, and at present there exist more than thirty SuperDARN radars covering considerable portions of high and mid latitude ionosphere in the northern and southern hemispheres. SuperDARN radars emit HF (8-20MHz) waves and receive echoes backscattered from either the ionosphere or the ground/sea. For the latter case, it is the most frequent that the emitted HF waves are reflected at the ionosphere, reaches the ground/sea, are backscattered there, and reaches back to the radar site along the same ray path (this is called a single-hop case; there could be

Manuscript received on 5 September 2016; accepted on 3 October 2016
* Department of Earth and Planetary Sciences, Faculty of Science, Kyushu University, 744 Motooka, Nishi-ku, Fukuoka 819-0395, Japan, and International Center for Space Weather Science and Education, Kyushu University, 744 Motooka, Nishi-ku, Fukuoka 819-0395, Japan
** National Institute of Polar Research, 10-3 Midori-cho, Tachikawa, Tokyo 190-8518, Japan, and Department of Polar Science, School of Multidisciplinary Sciences, SOKENDAI (The Graduate University for Advanced Studies), 10-3 Midori-cho, Tachikawa, Tokyo 190-8518, Japan
*** Department of Electronics and Control Engineering, Kitakyushu National College of Technology, 5-20-1 Shii, Kokuraminamiku, Kitakyushu, Fukuoka, 802-0985, Japan
**** Institute for Space-Earth Environmental Research, Nagoya University, Furo-cho, Chikusa-ku, Nagoya 464-8601, Japan
***** Present address: Department of Earth and Planetary Science, Graduate School of Science, The University of Tokyo, 7-3-1 Hongo, Bunkyo-ku, Tokyo 113-0033, Japan

cases with more reflections (for example, the HF waves that have reached the ground/sea are reflected there and reaches the ionosphere again), but such cases are less frequent than single-hop cases). The SuperDARN Hokkaido East radar is among those that were built first at mid-latitudes (Nishitani et al. 2011). Its field of view is shown at, e.g., http://cicr.isee.nagoya-u.ac.jp/hokkaido/site1/intro_e.html .

From the ionosphere-backscattered signals, one can obtain the Doppler velocity of the ionospheric plasma flow along the line of sight (LOS) of a radar beam. On the other hand from the ground/sea-backscattered signals, one can obtain the velocity of the vertical motion of the ionosphere, because it is the only variable that can change the ray path length of the single-hop signal: The ground/sea does not move much (compared to the ionosphere), and the horizontal velocity of the ionospheric plasma does not change the height of the ionosphere, thus does not change the ray path. The vertical velocity of the ionosphere is in general significantly smaller than the horizontal velocity, and one can judge the observed backscatter is a ground/sea backscatter if its Doppler velocity is less than ~50 m/s and its spectral width is less than ~50m/s (See Ribeiro et al. (2011) for more details).

Ponomarenko et al. (2003) showed that the ground/sea backscatters, observed by the SuperDARN TIGER radar located at ~ −55° AAGCM latitude in Tasmania, included continuous (lasting 4-5 hours a day on average) periodic oscillations, which they attributed to ULF waves. Among thus found events, Ponomarenko et al. (2005) showed a five-minute interval (embedded in the above-stated 4-5 hour interval) during which the latitude dependence of the power and the phase of the wave was consistent with those predicted from the field-line resonance (FLR) theory (Tamao 1965, Southwood 1974, Chen and Hasegawa 1974) which is summarized below. The resonance latitude of the FLR was estimated to be ~ −65° (i.e., L~6.0) in AACGM.

The FLR is the mechanism via which the fast-mode waves in the magnetosphere resonate with, and thus excite, eigenoscillations of the magnetospheric magnetic field lines. In other words, since the field-line eigenoscillations are maintained by the Alfven mode, the FLR is the mechanism in which the fast-mode waves are converted to the Alfven-mode waves, which can take place in an inhomogeneous plasma.

The FLR-generated Alfven-mode wave has characteristic latitude (on the ground) dependence of the amplitude and phase, as follows: For a fixed frequency, the amplitude shows a single peak at the latitude ("FLR latitude" below) where the (fixed) frequency is equal to the eigenfrequency of the field line there (the eigenfrequency is a function of latitude). On the other hand, the phase shows a monotonic change across the FLR latitude. (e.g., Southwood 1974).

The above-stated excitation of the field-line eigenoscillations via the FLR have been identified in ground magnetometer data (e.g., Samson et al. 1971, Kawano et al. 2002), satellite magnetic and electric fields data (e.g., Singer and Kivelson 1979, Liu et al. 2009), ground-based radar data (e.g., Fenrich et al. 1995, Ponomarenko et al. 2005, Nedie et al. 2012, Liu et al. 2013), and combination of these data (e.g., Rae et al. 2005).

The energy source of the FLR is, as stated above, fast-mode waves. As such fast-mode waves, azimuthally-propagating waves such as the Kelvin-Helmholtz waves are often considered (e.g., Southwood 1974, Chen and Hasegawa 1974; Fig. 7 of Glassmeier et al. (1999) is illustrative). On the other hand, cavity-mode waves, which are fast-mode radial eigenoscillations of a magnetospheric cavity, have also been considered as the energy source of the FLR (e.g., Fenrich et al. 1995). In the cavity mode, the plasma in the entire cavity radially oscillates with the same frequency. As the boundaries of the cavity region, the magnetopause (e.g., Kivelson and Southwood 1985, 1986), the plasmapause (e.g., Allan et al. 1986, Takahashi et al. 2010, and references therein), and the ionosphere have been suggested. When the outer (inner) boundary is the plasmapause (ionosphere), such a cavity is usually called the "plasmaspheric cavity" and it oscillates at frequencies in the order of 10 mHz (e.g., Takahashi et al. 2010, Chi et al. 2013); when the outer (inner) boundary is the magnetopause (ionosphere), such a cavity is often called the "global magnetospheric cavity" and it oscillates in the order of 1 mHz (e.g., Takahashi et al. 2010 and references therein).

In this paper we present a wave event identified in the ground/sea backscattered data obtained by the SuperDARN Hokkaido East radar, located in the mid-latitude area; its AACGM latitude (longitude) is 36.5° (214.7°). Our event, which took place at ~45° AACGM latitude (i.e., at L~2), had the following features, as shown in Section 3.

(C1) It did not have a long-lasting (4-5 hours) nature as reported by Ponomarenko et al. (2003, 2005), but continued for a relatively short time (about one hour), starting at the time of an SC on the ground.
(C2) The frequency of the observed wave was ~1 mHz, much smaller than the typically-observed frequency (in the order of 10 mHz) at L~2.
(C3) The one-hour event interval included a 16-minute interval which showed the amplitude and phase pattern the same as that of FLR-generated Alfven-mode eigenoscillations.

Items (C1) and (C3) are new findings in the mid-latitude area, and reports on item (C2) are limited in literature. The details will be presented below.

2. Data

In this paper we study the above-stated wave event observed by the SuperDARN Hokkaido East radar. We will first make a visual inspection of the SuperDARN data of this event, including comparisons with simultaneous solar wind data and geomagnetic data. We will then perform spectral analyses of the SuperDARN data. Finally we will discuss and summarize the obtained results.

The event of this paper took place on Aug. 19, 2009; on this day, the SuperDARN Hokkaido East radar was run in a mode in which the cadence of each beam observation was 60 seconds and the field of view (FOV) of each beam was divided into 220 range gates (RGs) in the radial direction with the range resolution of 15 km and with the first RG having the distance of 135 km from the radar (for the case of ionospheric echoes). Figure 1(b) shows VLOS (the velocity along the LOS, defined to be positive when the beam's reflector is approaching the radar site) along Beam 05, which had an angle of about 17° from the magnetic meridian at RG 91. (Fig. 1(a) and (c), showing Beam 00 and 10, will be discussed in Section 3.) In Fig. 1(b), the above-stated possible FLR took place at 10:26~10:42UT near this RG 91; more details will be described and discussed in Section 3. Almost all the data shown in Fig. 1 had VLOS's smaller than 50m/s in magnitude and are classified as ground/sea backscattered signals. The white parts in this figure corresponds to RGs which received no backscattered signal.

As the simultaneously observed solar wind data, we use 64-sec resolution ACE data, downloaded from CDAWeb (http://cdaweb.gsfc.nasa.gov/istp_public/). Details of the ACE data are discussed in Section 3.

We also use the data of the geomagnetic indices AE and SYM-H provided by the World Data Center for Geomagnetism, Kyoto (http://wdc.kugi.kyoto-u.ac.jp/). The AE index is that for substorm activities, and the SYM-H index can be regarded as a one minute-resolution version of Dst, which is an hourly index, widely used to define the magnitudes of magnetic storms. Some more detail on SYM-H/Dst is that it is the ground equatorial magnetic field deviation from its quiet-time value, and the deviation is caused by an increased ring current during storms. More details on AE and SYM-H/Dst are presented at the above website.

We also use ground magnetometer data from SuperMAG and Kakioka Magnetic Observatory of the Japan Meteorological Agency; details will be presented below. We will compare them with the SuperDARN data.

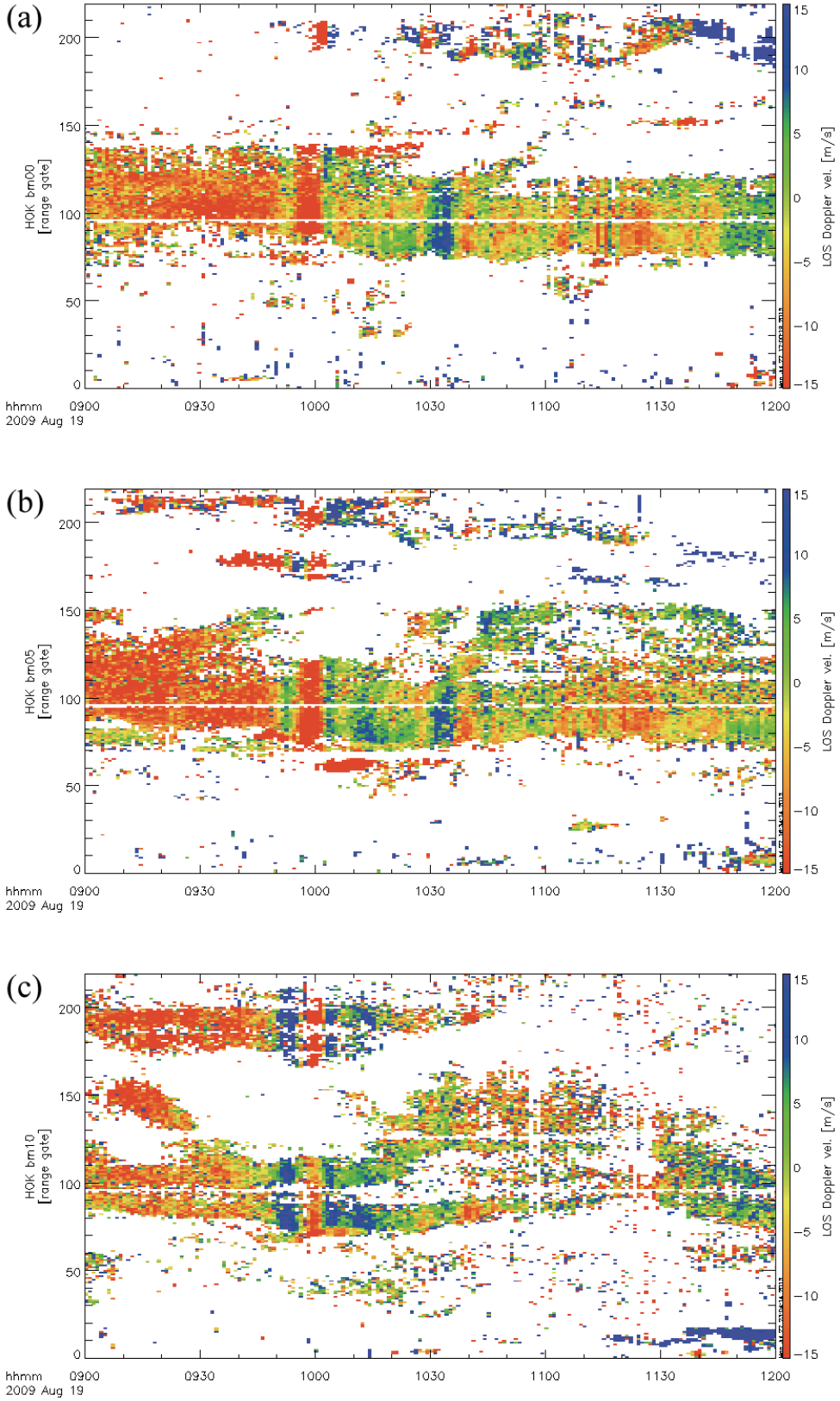

Fig. 1. Shows the line-of-sight Doppler velocity (VLOS) observed by Beam 00 (Panel a), 05 (Panel b), and 10 (Panel c) of the SuperDARN Hokkaido East radar at 09:00~12:00UT on Aug. 19, 2009. The time resolution is one minute. The vertical axis shows all the range gates (RGs). Note that the negative (positive) VLOS is painted in reddish (bluish) color. See text for more details.

3. Data Analysis and Results

In Fig. 1(b) we can see a wide vertical red band centered around 09:58UT. Before this red band, there is a narrower green vertical band starting at around 09:50UT. After these bands, we can visually identify at least six bands with similar horizontal width (i.e., time length) before 10:50UT. Since these bands alternately change their colors between reddish and bluish (negative (positive) VLOS is painted in reddish (bluish) color), it can be said that they have the nature of a wave, although their periodicity is rather irregular. Before 09:50UT and after 10:50UT, a similar band structure is not recognizable.

We also notice in Fig. 1(b) that the bands show a clear bending feature during the 10:26~10:42UT interval; this corresponds to the possible FLR feature we mentioned above. Further details will be described below.

Figure 2 shows the 64-sec solar wind data from the ACE spacecraft, and 1-min geomagnetic indices: From top, IMF Bz, the solar wind dynamic pressure (Pdyn), AE, and SYM-H are shown. The ACE data is shifted in time by 44 minutes, and as a result, Pdyn starts to make a clear and significant increase at about the same time as the SC identified in SYM-H (i.e., 09:50UT). To support this number 44, we have estimated the propagation lag for all the ACE data in the 44 minutes preceding 09:50UT (in Fig. 2) by using the following equation: (X·By-Y·Bx)/(-Vx·By+Vy·Bx), where all the quantities (X, Y: position, B: magnetic field, V: plasma velocity, all in GSE) are the data at ACE. This equation is a simplified version of that used by Lockwood et al. (1989), and shows the time lag for a straight IMF field line to convect from the ACE position to the position of the Earth center (in case there is no magnetospheric obstacles). At 09:06UT X was 244 Re and Y was 33 Re, thus the separation of ACE from the Sun-Earth line was not ignorable. As a result of the above calculation, we have obtained the median value of 120 min, with its 50±34.13 percentile range (which corresponds to the standard deviation range for normal distributions) of 40~342 min. That is, this range includes the above 44 min. Furthermore, during this 40~342 min interval, there was only one step-like increase in Pdyn from a quiet level (which is the one shown in Fig. 2); Thus, from the cause-and-effect point of view, it is the most reasonable to associate it with the SC starting at 09:50UT (identified in the SYM H data; see Fig. 2). It is also likely that the step-like increase in Pdyn also excited the waves in VLOS starting ~09:50UT (Fig. 1(b)); further support of this association with SC is presented just below.

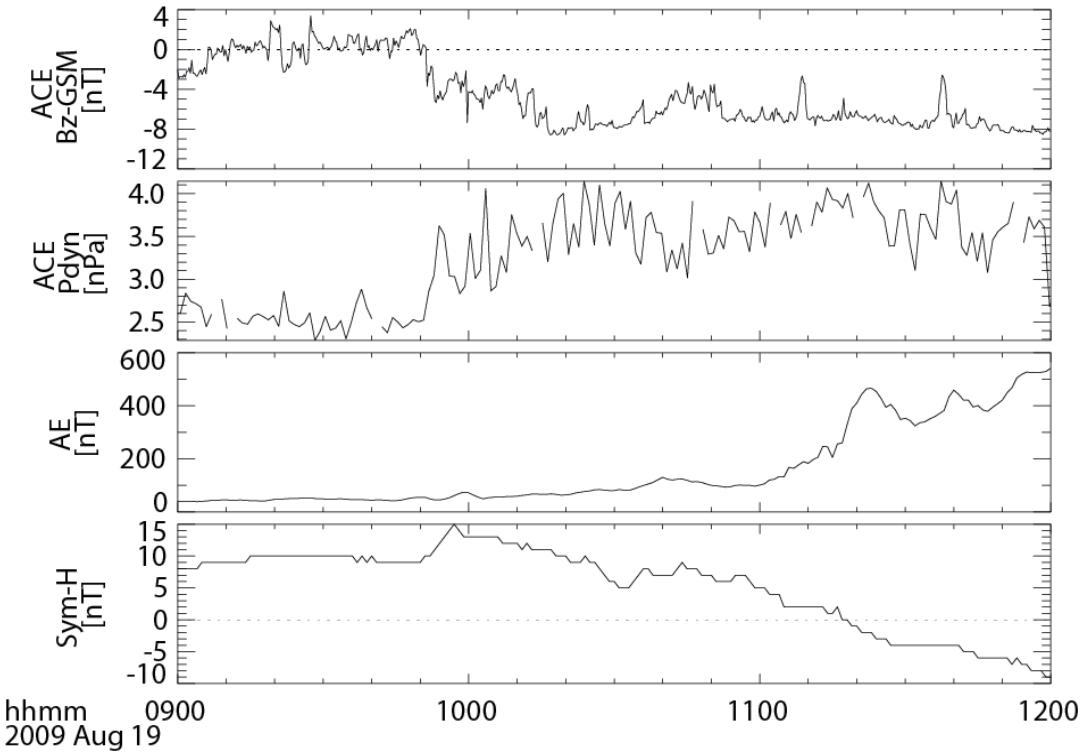

Fig. 2. Shows, from top, the IMF Bz [nT], the solar wind dynamic pressure [nPa], the AE index [nT], and the SYM H index [nT] for the same time interval as Fig. 1. The solar wind propagation lag is corrected. See text for more details.

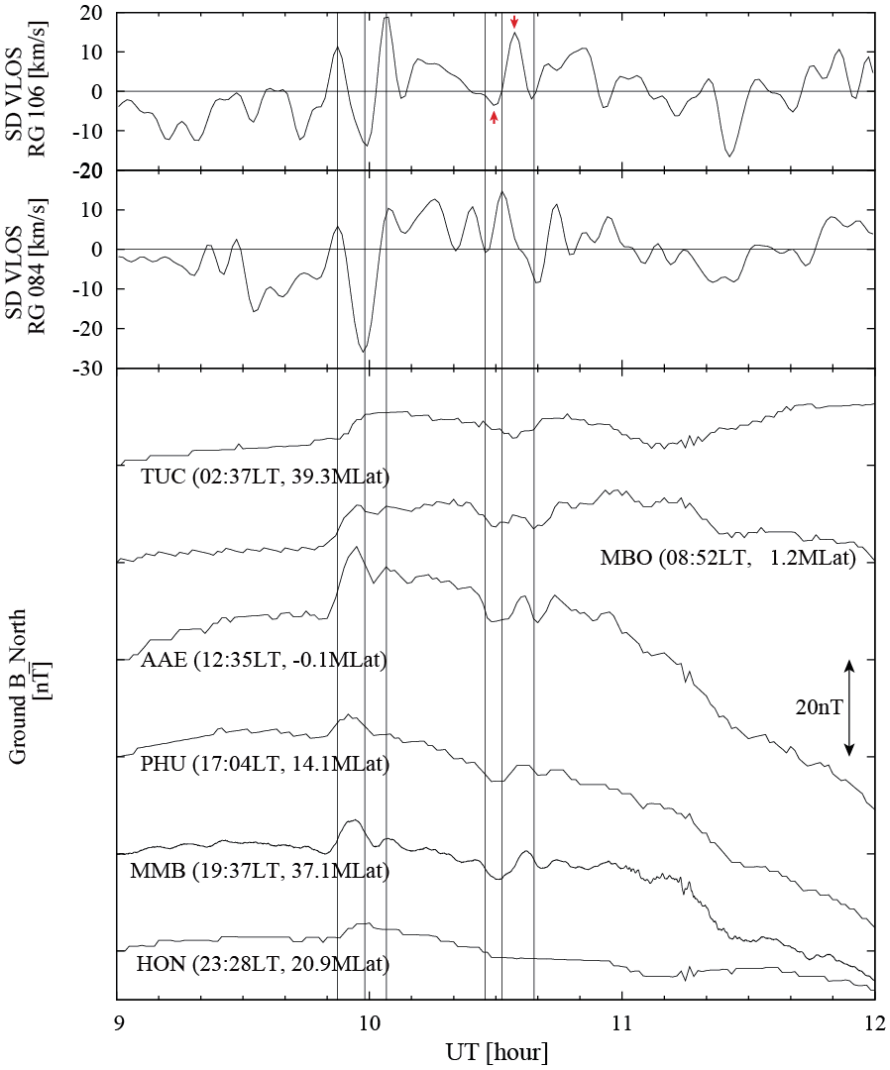

Fig. 3. Shows, from top, SuperDARN VLOS of RG106 (running through the upper part of the bending bands around 10:30UT in Fig. 1(b)), VLOS of RG84 (running through the lower part of the same bands), and mid- to low-latitude ground magnetometer data located at a wide range of longitudes (The local times shown in the legend are those at 10:00UT). See text for more details.

Figure 3 shows, from top, VLOS of RG106 (running through the upper part of the bending bands around 10:30UT in Fig. 1(b)), VLOS of RG84 (running through the lower part of the same bands), and mid- to low-latitude ground magnetometer data located at a wide range of longitudes (the local times shown in the legend are those at 10:00UT). These ground magnetometer data come from SuperMAG, except for the MMB data from the Kakioka Magnetic Observatory of the Japan Meteorological Agency. The time resolution of the SuperMAG (MMB) data shown in Fig. 3 is one minute (one second). We selected mid- to low-latitude stations to better identify compressional components. Shown in the figure is the northward component ("N component" below) of the magnetic field vector. Magnetic longitudes and latitudes [deg] of the stations in Fig. 3 are as follows: TUC: (−43.96, 39.32), MBO: (58.44, 1.2), AAE: (111.51, −0.06), PHU: (178.77, 14.11), MMB: (−143.33, 37.08), and HON: (−89.1, 20.88).

The VLOS data in this figure are bandpass-filtered (BPF'ed) with the period range of 320 seconds to six hours: The 320 seconds corresponds to the central frequency of the fourth-left column of Fig. 5, so that the frequency range of the BPF includes the frequencies of the leftmost three columns for which the wave power was relatively large (details of Fig. 5 will be explained below), and the six hours is twice the time length of Fig. 3. No bandpass filtering has been applied to the ground magnetometer data.

Except near the local midnight, the perturbations in the ground magnetometer data are commonly and simultaneously observed, and had the frequency of ~1mHz, suggesting that these are global magnetospheric cavity-mode waves (e.g., Kivelson and Southwood 1985, 1986). We also note that the initial biggest perturbations starting around 09:50UT are likely to correspond to the SC.

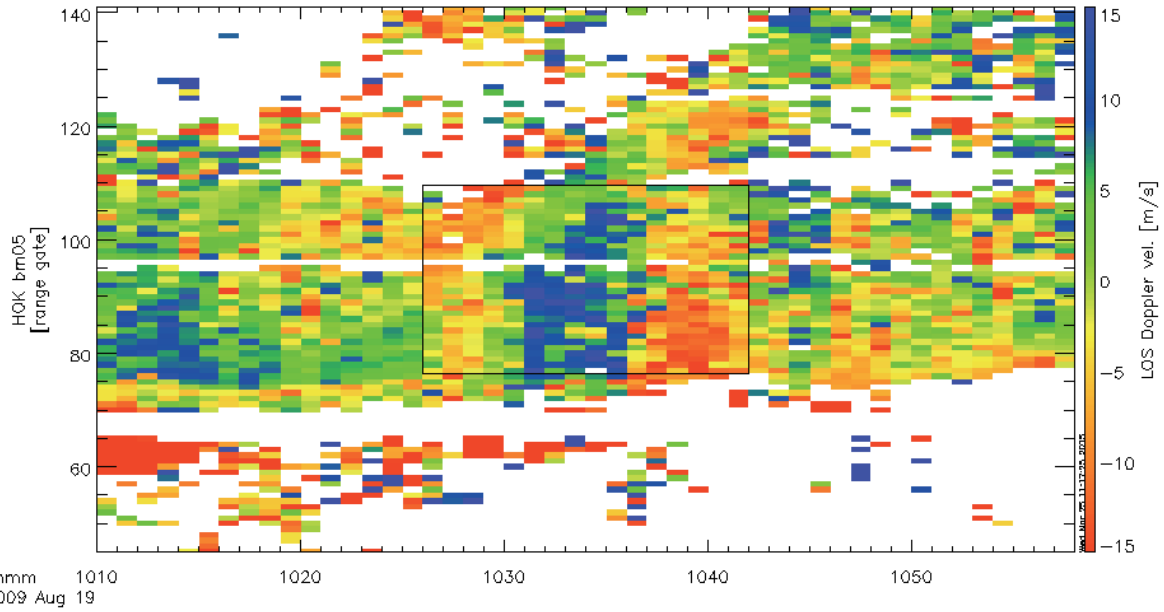

Fig. 4. Shows a closeup of Fig. 1(b), and the superposed black rectangle (corresponding to 10:26~10:42UT and RG=77~109) indicates the wave bands that are bending. For each RG, all the 16 timeseries data in the rectangle (corresponding to a row in the rectangle) are Fast Fourier Transformed (FFT'ed). See text for more details.

Vertical lines in the figure run through maxima and minima in the SuperDARN VLOS at RG 84. In general, the VLOS was at maximum (minimum) when the ground N component was increasing (decreasing). This feature can be explained as follows: For ground/sea echoes, an increase (decrease) in VLOS actually reflects the vertical downward (upward) motion of the ionosphere where the echoes are reflected, because it decreases (increases) the length of the ray path between the radar site and the ground/sea backscattering point. The downward (upward) motion of the ionosphere is caused by the compression (rarefaction) of the magnetosphere via the fast mode waves: Differently put, this compression (rarefaction) corresponds to the westward (eastward) wave electric field which causes, with the tilted field line topology, the downward (upward) motion of the ionosphere.

At ground high latitudes, magnetic pulsations starting just after SCs, having frequencies similar to the above-mentioned waves of this paper, have been reported (e.g., Araki et al. 1997) and have sometimes been referred to as Psc. However, at mid-latitudes, we do not know a previous paper which reported SC-triggered waves having frequencies similar to the waves of this paper.

We have noticed in Fig. 1(b) that the bands around 10:30UT bend toward the top right. Figure 4 is a closeup of Fig. 1(b), and the bending bands are surrounded by a black rectangle. Although the time resolution is rather coarse with this scaling, the bending feature is apparent in the middle blue band surrounded by the rectangle, clear enough for the leftmost red band, and barely identifiable for the rightmost red band. It is to be noted that the cavity mode cannot generate this bending feature by itself.

The right three vertical lines in Fig. 3 are drawn in the time range of the rectangle in Fig. 4. The red vertical arrows in the top panel of Fig. 3 show that the peaks at RG 106 were delayed from those at RG 84, (naturally) consistent with Fig. 4.

To further analyze this bending feature, we have performed the spectral analysis, as follows. Each RG yields timeseries data of VLOS, and for each of the RGs surrounded by the black rectangle in Fig. 4, that is, RG = 77~109, we have applied FFT to all of its timeseries data surrounded by the rectangle, that is, all of its VLOS data from 10:26UT to 10:42UT; this means applying FFT to 16 timeseries datapoints, because the data time resolution is one minute. We note we have applied no bandpass filter before applying the FFT. We also note we have applied the Hanning window before applying the FFT.

After applying the above-stated analysis procedure, we obtain, for each RG, the real and imaginary parts of the FFT results as functions of frequency. The frequency resolution is 1/16/60[s] = 1.042[mHz]. From the obtained real and imaginary parts, we can calculate the power and phase. Figure 5 shows thus obtained power as a function of frequency (horizontal axis) and RG (vertical axis). From this figure it is clear that the wave power is the largest at 1.042 mHz, or if we take into account the frequency resolution, that the wave power is the largest in the 0.521-1.563mHz range (corresponding to the second-left column of Fig. 5). Thus, in the following analyses to study the latitude dependence of the wave power and phase, we will use only the FFT results at 1.042 mHz.

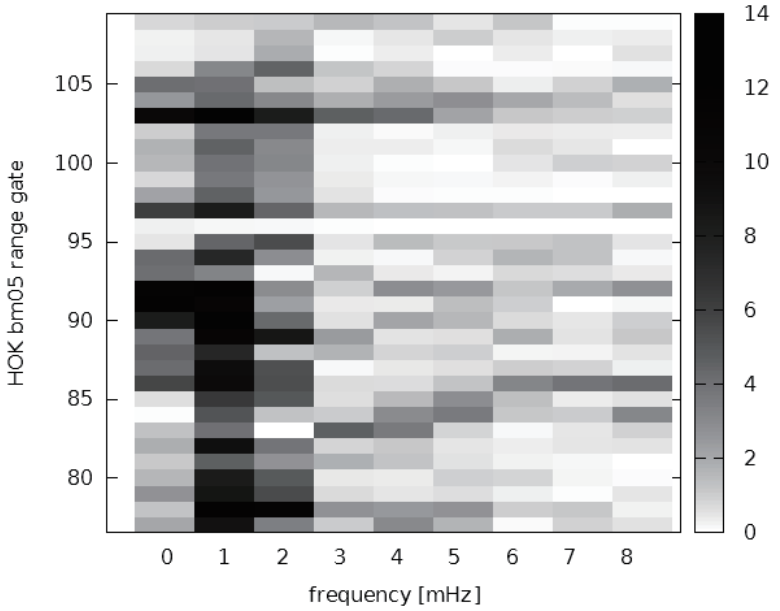

Fig. 5. Shows, by grey colors, the wave power obtained by applying the FFT to the data in the rectangle of Fig. 4. The horizontal axis shows the frequency, which has the 1.042mHz resolution. The vertical axis shows the RG numbers. See text for more details.

By fixing the frequency to 1.042 mHz, we obtain one value of the wave power (phase) for one given RG. Since the latitude increases with increasing RG number, we can study the latitude dependence of the wave power and phase by plotting them as a function of the RG number. The result of doing so is shown in Figure 6: The top panel shows the wave power, and the bottom panel shows the wave phase, as functions of the RG number (horizontal axis). Since the original FFT results are rather scattered as a function of the RG number (which is mainly because the original number of timeseries data are small (16)), we have smoothed the latitude profiles by moving-averaging the data from adjacent nine RG's, and the result is shown in Fig. 6.

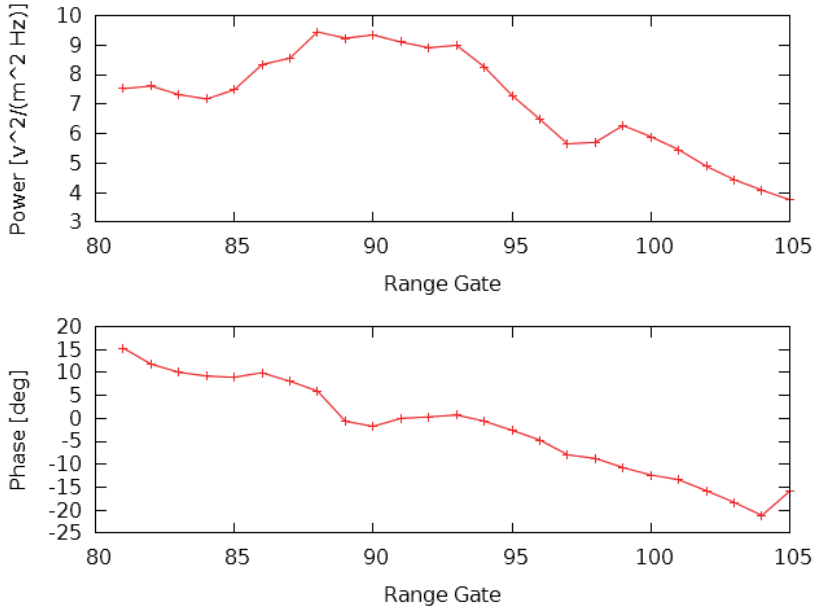

Fig. 6. From the FFT results, (top) the power and (bottom) the phase of the data at 1.042mHz (corresponding to the second-left column in Fig. 5) are shown as a function of the RG number. They are smoothed in the direction of the horizontal axis by moving-averaging nine adjacent data. In the bottom panel, a constant offset is subtracted from all the data so that the phase at RG 91 (center of the event) is zero. The combination of the two panels' patterns is consistent with FLR-generated waves. See text for more details.

4. Discussion

The essential features of the wave event of this paper observed at L~2 for 09:50~10:50UT are summarized as follows (they are more detailed version of what we wrote at the end of Section 1):

(C1) It was probably triggered by a step-like increase in Pdyn which reached the ionosphere around 09:50UT, and continued for a relatively short time (about one hour; see Figs. 1(b) and 2). These features are in contrast to the waves reported by Ponomarenko et al. (2003, 2005), which continued for 4-5 hours without clearly identifiable triggers.
(C2) This wave was observed by the SuperDARN Hokkaido East radar and by the mid- to low-latitude ground magnetometers in a synchronized manner (Fig. 3). The frequency of the observed wave was ~1mHz (Fig. 3), much smaller than the typically-observed frequency (in the order of 10 mHz) at L~2 (e.g., Takahashi et al. 2010, Chi et al. 2013).
(C3) The one-hour event interval included a 16-minute interval (10:26~10:42 UT; see Fig. 4) which showed the amplitude and phase pattern the same as that of FLR-generated Alfven-mode eigenoscillations (Fig. 6).

The SuperDARN Hokkaido East radar observed Items (C1) and (C3) for the first time as the mid latitude phenomena, and reports on item (C2) are quite limited in literature.

Item (C1) is self-explanatory and we do not have much to add at this point; we will refer to (C1) in the Summary section. We then proceed to discussing Item (C2). Fig. 1 shows that, except for the 16-min interval of 10:26~10:42UT (Item C3), the bands were vertical, meaning that the phase was the same at all the latitudes. This feature suggests that these waves (except for the waves in the above-mentioned 16-min interval) correspond to the cavity mode. However, as stated above, the typical frequency of the plasmaspheric cavity mode is in the order of 10 mHz (e.g., Takahashi et al. 2010, Chi et al. 2013). Thus, we interpret the frequency of our event (~1 mHz) at L~2 in terms of the global magnetospheric cavity-mode waves (Kivelson and Southwood, 1985, 1986) which has the same frequency in both the trough region and the plasmasphere. It is only such a global cavity mode that can have the frequency of ~1 mHz in the plasmasphere. On the other hand, observations of such a global mode are quite limited: Kokubun et al. (2013) is the only paper we are aware of. Thus, this paper constitutes a useful addition to the publication of such phenomena.

We next discuss Item (C3). Fig. 6 shows the results of the spectral analysis of the above-stated 16 min interval of 10:26~10:42UT, for RG = 77~109. It shows that the wave power has a maximum near RG 91, and that the phase continuously decreases with increasing RG (latitude) across RG 91. This combination of the power profile and the phase profile (as a function of latitude) is typically observed at the FLR (e.g., Pilipenko and Fedorov 1994, Fenrich et al. 1995, Kawano et al. 2002).

Here we note that, due to the resonance width (explained in the above references), the frequency dependence of the power and the phase becomes gradual, not showing a step-like change across the resonance point. In addition, the power of the FLR-generated wave is smaller at lower latitude (e.g., Chi et al. 2013). Thus, at mid-latitudes, it is often difficult to observe a full 180deg phase shift, because at distances from the FLR resonance point, the FLR signal becomes smaller than the background signal level; this signal-noise ratio effect is not included in the standard FLR theory.

If the amplitude-phase pattern observed at 10:26~10:42UT (Figs. 4-6) is caused by the FLR which couples the above-stated global magnetospheric cavity-mode waves with the Alfven-mode eigenoscillations, another expected feature is that the FLR frequency increases with decreasing latitude, because the field line length becomes shorter and enables quicker eigenoscillations of the field line (although the cavity-mode frequency is essentially the same inside the cavity, it has a finite frequency range (half width) like any natural phenomena, and the FLR-generated Alfvenic eigenfrequency changes within that finite frequency range). Fig. 5 appears to support this; that is, at small RG numbers, the wave power is large not only at 1.042 mHz but also at 2.083mHz (see the RG numbers less than ~90 in the third-left column).

If we regard this pattern during the interval 10:26~10:42 UT as a result of the FLR, what is not typical about this interval is that the FLR generated poloidal-mode Alfven waves in this interval while the most of the previously identified FLR events were associated with toroidal-mode Alfven waves (e.g., Fenrich et al. 1995, Sakaguchi et al. 2012). In the following we will call the former case “poloidal FLR” and the latter case “toroidal FLR” for simplicity, and describe more details of them, starting with the “toroidal FLR” and then the “poloidal FLR.”

The toroidal FLR couples magnetopause surface waves (such as the Kelvin-Helmholtz waves), which

propagate tailward and radially inward via the fast mode, to toroidal-mode Alfven waves (Fig. 7 of Glassmeier et al. (1999) is illustrative). The generated toroidal-mode Alfven waves move (i.e., cause the **E**×**B** drift of) the ionospheric plasma in the east-west horizontal direction (not in the vertical direction), meaning that the ray path length between the radar and the backscattering region on the ground/sea does not change and thus that the VLOS is unchanged, regardless of the beam direction. In more detail, since SuperDARN estimates the location of a reflector of a radar beam (i.e., an HF wave beam) by dividing the ray path length by the beam speed, no change in the ray path length means no motion of the reflector and thus no change in the VLOS. Thus, ground/sea backscattered signal shows no wavy perturbation when toroidal-mode Alfven waves take place.

On the other hand, the poloidal FLR couples fast-mode waves (including the cavity modes mentioned above) to poloidal-mode Alfven waves, and thus-generated poloidal-mode Alfven waves vertically move the ionosphere, because the magnetic field line (which oscillates radially in the magnetosphere) is tilted in the mid- to low-latitude ionosphere. Therefore, the poloidal-mode Alfven waves can change the beam's ray path length, and thus can change the VLOS. We note Ponomarenko et al. (2005) also interpreted that the FLR-generated Alfvenic pulsations which they observed in the ground/sea backscattered signals were in the poloidal mode. As stated above, the vertical bands in Fig. 1(b) are likely to have been caused by the cavity mode; thus, their bending (Fig. 4) suggest the coupling of the cavity-mode waves and the poloidal-mode Alfven waves, since the cavity mode cannot bend the bands by itself.

In this paper we have analyzed Beam 05 only, but Beams 02 through 06 showed more-or-less similar features (not shown). These beams had the angles from the magnetic meridian from 7° (Beam 02) to 21° (Beam 06). For larger beam numbers (referring to more eastside beams in the field-of-view of the radar, looking at lower latitudes), the three bands marked in Fig. 4 became less clear (data of Beam 08 is shown in Fig. 1(c)). A possible reason for this is as follows: The ground/sea backscatters tended to be observed at similar RG ranges for many beams (not shown), which means that the eastside beams (having larger angles to the magnetic meridian) observed ground/sea backscatters at lower latitudes than the westside beams; then, if the FLR effect (taking place at similar latitudes) enhances the wave bands in some manner, the eastside beams were reflected at latitudes lower than the latitudes of the enhanced wave bands, thus missed the bands.

On the other hand for smaller beam numbers (i.e., Beam 00 and 01, having the angles from the magnetic meridian of 1° and 4°), the three bands at 10:26~10:42UT (corresponding to the central rectangular in Fig. 4) did not show a clear bending shape but were fairly straight in the vertical direction (data of Beam 00 are shown in Fig. 1(a)). A possible reason for this is as follows: As stated above, we think that the straight vertical parts of the bands in Fig. 1(b) are the result of the global magnetospheric cavity-mode oscillations (Kivelson and Southwood, 1985, 1986), that the FLR in the 10:26~10:42UT interval coupled the cavity-mode wave and the poloidal-mode Alfven wave, and that the generated Alfven wave yielded the bending feature clearly seen around RG 91 in the central rectangle of Fig. 4. Then, the no-bending feature of the same bands for Beam 00 and 01 may mean that FLR was not active there. (The change in the band shape for Beam 01 through Beam 05 was not abrupt but more-or-less gradual (not shown).) It is generally thought that the FLR structure has a large east-west size, but we note that Fig. 2(d) of Sakaguchi et al. (2012) shows that FLR-driven Pc5's at high latitude were observed at 20MLT but not at 19MLT. Further understanding of the longitude-dependent feature (of our mid-latitude event) needs statistical analyses of more events, which is a topic of future research.

Returning to the bending feature of the VLOS bands, if we regard the observed pattern as a result of the FLR, then the observed wave frequency can be used to estimate the equatorial plasma mass density along the field line which is under the FLR; this field line ran through RG 91 for the event of this paper. The L value of RG 91 is L = 1.992 (corresponding to the AACGM magnetic latitude of 44.88°).

There are many methods for the estimation, and in this paper we use the method of Singer et al. (1981) which is a general method that can calculate the poloidal-mode eigenfrequency for any magnetic-field model and any plasma-density model. The method numerically solves the differential equation of Alfven waves to obtain the eigenfrequency (for more details, refer to Singer et al.). As the magnetic field model input into this method, we use the Tsyganenko 05 model (Tsyganenko and Sitnov, 2005). As the plasma density model input into this method, we use the following model:

$\rho = \rho_0 \left(\frac{La}{r}\right)^m$, where L is the L value, a is the Earth radius, r is the radial distance of any point along the field line in question, m is a parameter usually pre-defined, and ρ_0 (the quantity to obtain, the only one unknown parameter) is the equatorial mass density of the field line. This functional form is quite popularly used, and there are many studies on the proper value of m; in this paper we follow Goldstein et al. (2001) and set m to 1.17; they obtained this number by using the plasma wave data observed by the Polar spacecraft in the L range from 2.5 to 6.3. This L range barely misses 1.992 for our event, but to our knowledge it is the closest. We note here that Chi et al. (2000) and Takasaki et al. (2006) used m = 4 for ground-based observations at L = 2 and 1.4, respectively. Chi

et al. (2000) did not mention what let them use this number. Takasaki et al. (2006) used $m = 4$ so that their analysis procedure would be consistent with Chi et al. (2000). Takahashi et al. (2004) made a detailed study on the value of m by using spacecraft data, and they obtained $m = 0.5$ for $4 \leq L < 6$; this number is popularly used at present, but the spatial coverage of Takahashi et al. (2004) was $L = 4$ at minimum. We also note that Obana et al. (2015) used $m = 1$ for their density estimation at $L = 2.33$. To our knowledge there is no paper which changed the value of m depending on the storm or SC activities. The actual procedure to obtain ρ_0 is to search for ρ_0 so that the calculated eigenfrequency (by inputting the ρ_0 to the Singer et al.'s method) equals to the actually observed frequency (for more details, refer to Singer et al.).

As stated above, the observed wave frequency is in the range of 0.521-1.563 mHz, with the center being 1.042 mHz. In the following we use 1.563 mHz, because visual inspection of Fig. 4 suggests that there are 1.5 wave periods in the rectangle having the time length of 16 minutes; the frequency calculated from these numbers equals to 1000/(16×60/1.5) = 1.563 [mHz].

By inputting this 1.563 (mHz, as the poloidal eigenfrequency) and 1.992 (as the L value) into Singer et al.'s method, we obtain 2.643×10^5 amu/cm^3 as the equatorial density ('amu' refers to the atomic mass unit, using which one H^+ is counted as one, one He^+ is counted as four, one O^+ is counted as 16, etc.). Since the electron number density at $L = 1.992$ is usually in the order of 10^4/cm^3 (for example, in Fig. 3 of Gallagher et al. (2000) which shows the direct density observations by spacecraft at $Kp < 1.3$, the maximum density at L~2.1 is ~1.3×10^4/cm^3), this number 2.643×10^5 appears unrealistic at first sight.

There are four factors which could explain the above-stated large density, as follows:

(E1) In the 10:26~10:42UT interval, the global cavity-mode waves were coupled to quarter-wave-mode (not fundamental-mode) poloidal Alfven waves (eigenoscillations) via the FLR. With this, the density estimated from the observed wave frequency (i.e., 1.563 mHz) has the same order as those in past satellite observations at L~2.
(E2) The compression of the plasmasphere by the sudden increase in Pdyn at the time of the SC directly increased the plasma density in the plasmasphere.
(E3) The compression of the ionosphere by the increased Pdyn yielded, as a reaction, ionospheric heavy ion outflow to the plasmasphere.
(E4) Ionospheric heavy ion outflow to the plasmasphere was enhanced as the effect of the magnetic storm main phase.

(E2) is so straightforward that we do not have further discussion on it. The other three factors are described in more detail just below. It is possible that all these four factors took effect during the event of this paper, and the combination of these four effects have a good chance of explaining the observation. (In addition to these four factors, we have considered the possible effect of the deformation of the magnetic field at L~2 due to the enhanced ring current during the storm. Takasaki et al. (2006) estimated how much field lines (at L~1.4) were deformed during their storm event, having Dst = −300 [nT], by using the Tsyganenko 05 model. The estimated changes in the field-line length and the equatorial magnetic field strength were both less than 1%. From this, although our observation was made at L~2, i.e., larger than 1.4, we think the effect of the deformation of the magnetic field was small.)

(E1) Quarter waves (Obana et al. 2008) take place near the dawn and the dusk: On the dayside, the ionospheric conductance is large due to the sunlight, and the both ends of the field line are nodes because the ionospheric currents associated with the wave tend to stop the motion of the field line there. On the other hand near the dawn and the dusk, it can happen that one end is on the dayside and the other end is on the nightside. The ionospheric conductance is small on the nightside, and thus the nightside end is an antinode. This leads to the quarter wave.

The above means that, while the wavelength of the fundamental-mode Alfven wave (eigenoscillation) is twice the field-line length, the wavelength of the quarter wave is four times the field-line length. Thus, the quarter-wave frequency is about half of the fundamental-mode eigenfrequency; this is analogous to the fact that the second harmonic-mode eigenfrequency is about twice the fundamental-mode eigenfrequency.

Our event took place around 10:30UT, which is 19:30LT, i.e., near the dusk. Thus, it is possible that the observed waves were quarter waves; if we employ this possibility, the fundamental-mode eigenfrequency is about 3.1 mHz (twice the observed frequency 1.563 mHz), leading to the density of about 6.6×10^4 amu/cm^3, i.e., one fourth of the above-obtained 2.643×10^5 amu/cm^3 (because the eigenfrequency is roughly proportional to the inverse of the Alfven-wave travel time along the field line, and because the Alfven speed is proportional to the inverse of the square root of the density). This 6.6×10^4 amu/cm^3 is in the same order as the usual density range at $L = 1.992$ near 10^4 amu/cm^3; as we mentioned above, Fig. 3 of Gallagher et al. (2000) shows that, even during

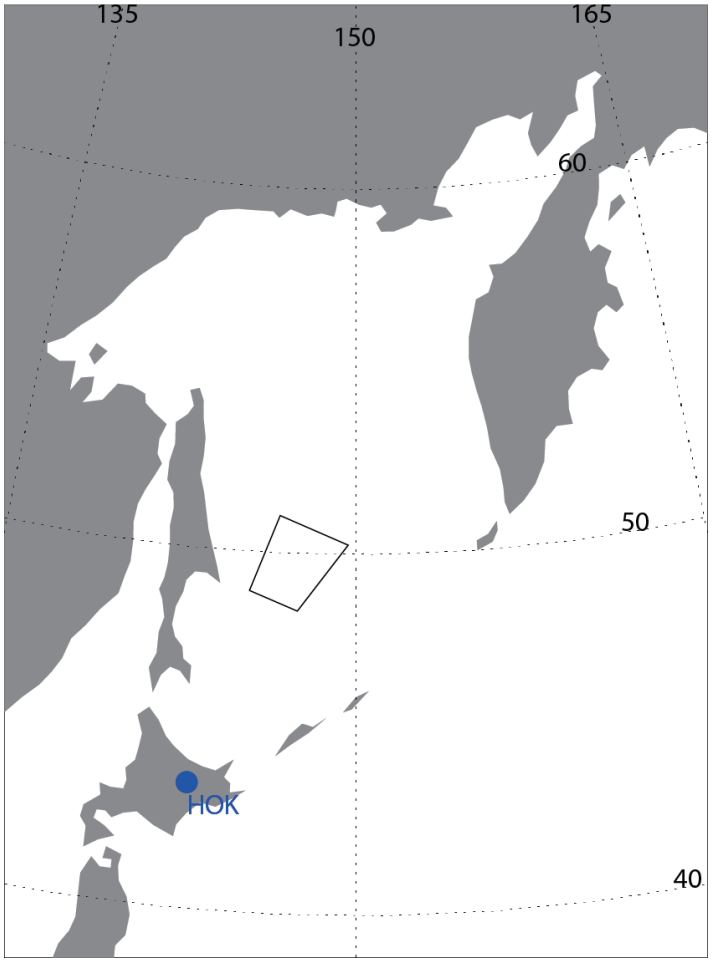

Fig. 7. Shows the area where the bending of the band of VLOS (i.e., the possible signature of FLR) was observed. It was observed by Beam 02 through 06, and for RG 77 through 109, at 10:26~10:42UT. This figure shows this area near the central time of the event duration.

geomagnetically quiet intervals, the maximum density directly observed by spacecraft at L~2.1 is ~1.3×10^4/cm^3.

Here one may think 19:30LT is well in the nightside. So that the quarter waves take place along a field line, the conductance difference between the two footpoints of the same field line is important, and the sunlight increases the conductance. Obana et al. (2015) estimated the ratio of the interhemispheric Pedersen conductance and the same-definition ratio of the Hall conductance for observed quarter waves, and suggested the threshold of five for the both quantities above which quarter waves could take place.

To address this issue, we have first identified the area where the bending of the band of VLOS (i.e., the possible signature of FLR) was observed. As stated above, it was observed by Beam 02 through 06, and for RG 77 through 109, for 10:26 to 10:42UT. Figure 7 shows this area near the central time of the event duration.

Then, by using the IRI model (Bilitza et al. 2011) for the ionosphere and the NRLMSISE-00 model for the atmosphere (Piscone et al. 2002), we have calculated the height-integrated (80-500km) Pedersen and Hall conductance values at the central point of this possible FLR area as shown in Fig. 7 at the event time, and obtained 0.47mho and 0.33mho, respectively. We have also calculated the same-definition conductance values at the conjugate point, and obtained the Pedersen (Hall) conductance value of 0.13mho (0.13mho). Thus, the interhemispheric Pedersen and Hall conductance ratios are 3.7 and 2.5. The former value is close to five. Thus we think that the possibility of the quarter wave is not negligible for the event of this paper.

(E3) We note that Kale et al. (2009) reported an increase in the plasmaspheric density just after an SC; they attributed it to the ionospheric O^+ outflow to the plasmasphere, as a result of the ionospheric density enhancement due to the ionospheric compression by the increased Pdyn. The O^+ outflow increases the plasmaspheric ion amu density much larger than the electron number density (if all the ions are H^+, then the ion amu density is equal to the electron number density). It is quite possible that the same effect took place for the event of this paper.

(E4) SYM-H increased at SC and then decreased (Fig. 2, bottom panel), indicating a magnetic storm (it was a

very small storm, with SYM-H reaching its minimum value −26nT at 19:48~19:50UT on this day, but having the time profile of SYM-H (Dst) typical to storms (not shown; readers are referred to the website of the WDC Kyoto and/or OMNIweb for the plots)). In the possible FLR interval (10:26~10:42UT), SYM-H was on the decreasing trend (Fig. 2. bottom panel, from ~10:00UT to the rightside edge of the figure), meaning the enhancement of the ring current, a typical feature of the storm main phase; this is also supported by the simultaneously observed continuously negative IMF Bz (Fig. 2, top panel), which in general leads to a ring current buildup. Then, we note Takasaki et al. (2006) reported a case in which the mass density at L~1.4 was increased during a magnetic storm. As its cause, they suggested an outflow of heavy ions (e.g., O^+) from the ionosphere as a result of the enhanced ionospheric activity due to precipitating particles and enhanced FACs.

5. Summary

Many waves have been observed in the ground/sea backscattered signals of mid-latitude SuperDARN radars, but past reports mainly looked at waves lasting for a long time. In this paper we have reported for the first time in the mid latitudes a relatively short-living wave after an SC and during the following magnetic storm. It may constitute a distinct category with unique characteristics, such as having a small wave frequency and including FLR interval(s) associated with an increased mass density. It is a topic of future research to conduct a statistical analysis of this type of events to clarify its nature, including what controls the occurrence of ~1 mHz waves and what controls the duration of the waves after SCs (about one hour for the event of this paper). It is also a topic of future research to study data from ground magnetometers near the event location.

6. Acknowledgements

This research was supported by the National Institute of Polar Research through its General Collaboration Projects no.24-11, 25-7 and 26-8. We would like to thank all the staff who contributed to the managements and operations of the SuperDARN Hokkaido East radar. This research was also supported by Special Funds for Education and Research (Energy Transport Processes in Geospace) and IUGONET project of the Ministry of Education, Culture, Sports, Science and Technology of Japan. The computer software package UDAS, which later became a part of SPEDAS, was made in the IUGONET project and is used in this work, and we appreciate it. The fitacf CDF data and the data analysis software of the SuperDARN Hokkaido East radar were distributed by ERG-Science Center (ERG-SC) operated by ISAS/JAXA and ISEE/Nagoya University, and the work of T. H. was done at ERG-SC. We acknowledge use of NASA/GSFC's Space Physics Data Facility's CDAWWeb service, and the ACE spacecraft data obtained from it. We also acknowledge use of the AE and Dst indices distributed by the World Data Center for Geomagnetism, Kyoto. For the MMB ground magnetometer data we gratefully acknowledge the Kakioka Magnetic Observatory of the Japan Meteorological Agency. For the other ground magnetometer data used in this paper we gratefully acknowledge: Intermagnet; USGS, Jeffrey J. Love; CARISMA, PI Ian Mann; CANMOS; The S-RAMP Database, PI K. Yumoto and Dr. K. Shiokawa; The SPIDR database; AARI, PI Oleg Troshichev; The MACCS program, PI M. Engebretson, Geomagnetism Unit of the Geological Survey of Canada; GIMA; MEASURE, UCLA IGPP and Florida Institute of Technology; SAMBA, PI Eftyhia Zesta; 210 Chain, PI K. Yumoto; SAMNET, PI Farideh Honary; The institutes who maintain the IMAGE magnetometer array, PI Eija Tanskanen; PENGUIN; AUTUMN, PI Martin Conners; DTU Space, PI Dr. Jürgen Matzka; South Pole and McMurdo Magnetometer, PI's Louis J. Lanzarotti and Alan T. Weatherwax; ICESTAR; RAPIDMAG; PENGUIn; British Artarctic Survey; McMac, PI Dr. Peter Chi; BGS, PI Dr. Susan Macmillan; Pushkov Institute of Terrestrial Magnetism, Ionosphere and Radio Wave Propagation (IZMIRAN); GFZ, PI Dr. Jürgen Matzka; MFGI, PI B. Heilig; IGFPAS, PI J. Reda; University of L'Aquila, PI M. Vellante; SuperMAG, PI Jesper W. Gjerloev. We used a webpage at Kyoto University, Japan (http://wdc.kugi.kyoto-u.ac.jp/ionocond/sigcal/index-j.html), to calculate the ionospheric conductance, and are grateful for it. We also appreciate S. Abe and S. Imajo for providing computer programs used in this study. Thanks are due to Dr. Kentarou Kitamura at the National Institute of Technology, Tokuyama College who reviewed this paper.

7. References

Allan, W., Poulter, E.M. and White, S.P. (1986) Hydromagnetic wave coupling in the magnetosphere: Plasmapause effects on impulse - excited resonances, *Planet. Space Sci.*, **34**, 1189-1220, doi:10.1016/0032-0633(86)90056-5.

Araki, T., Fujitani, S., Emoto, M., Yumoto, K., Shiokawa, K., Ichinose, T., Luehr, H., Orr, D., Milling, D.K., Singer, H., Rostoker, G., Tsunomura, S., Yamada, Y. and Liu, C.F. (1997) Anomalous sudden commencement on March 24, 1991, *J. Geophys. Res.*, **102**(A7), 14075-14086, doi:10.1029/96JA03637.

Bilitza, D., McKinnell, L.-A., Reinisch, B. and Fuller-Rowell, T. (2011) The International Reference Ionosphere (IRI) today and in the future, *J. Geodesy*, **85**, 909-920, DOI 10.1007/s00190-010-0427-x.

Chi, P.J., Russell, C.T., Musman, S., Peterson, W.K., Le, G., Angelopoulos, V., Reeves, G.D., Moldwin, M.B., and Chun, F. K. (2000) Plasmaspheric depletion and refilling associated with the September 25, 1998 magnetic storm observed by ground magnetometers at $L = 2$. *Geophys. Res. Lett*, **27**(5), 633-636.

Chi, P.J., Engebretson, M.J., Moldwin, M.B., Russell, C.T., Mann, I.R., Hairston, M.R., Reno, M., Goldstein, J., Winkler, L.I., Cruz-Abeyro, J.L., Lee, D.-H., Yumoto, K., Dalrymple, R., Chen, B., and Gibson, J.P. (2013) Sounding of the plasmasphere by Mid-continent MAgnetoseismic Chain (McMAC) magnetometers, *J. Geophys. Res.*, **118**, 3077-3086, doi:10.1002/jgra.50274.

Chen, L. and Hasegawa, A. (1974) A theory of long-period magnetic pulsations, 1, Steady state excitation of field line resonance, *J. Geophys. Res.*, **79**:1024-1032.

Fenrich, F.R., Samson, J.C., Sofko, G., and Greenwald, R.A. (1995) ULF high- and low-m field line resonances observed with the Super Dual Auroral Radar Network, *J. Geophys. Res.*, **100**, 21535-21547.

Gallagher, D.L., Craven, P.D., and Comfort, R.H. (2000) Global core plasma model, *J. Geophys. Res.*, **105**:18819-18833. doi:10.1029/1999JA000241.

Gjerloev, J.W. (2012) The SuperMAG data processing technique, *J. Geophys. Res.*, **117**, A09213, doi:10.1029/2012JA017683.

Gjerloev, J.W. (2009) A Global Ground-Based Magnetometer Initiative, *EOS*, **90**, 230-231, doi:10.1029/2009EO270002.

Glassmeier, K.H., Othmer, C., Cramm, R., Stellmacher, M., and Engebretson, M. (1999) Magnetospheric Field Line Resonances: A Comparative Planetology Approach, *Surv. Geophys.*, **20**(1), 61-109.

Goldstein, J., Denton, R.E., Hudson, M.K., Miftakhova, E.G., Young, S.L., Menietti, J.D., and Gallagher, D.L. (2001) Latitudinal density dependence of magnetic field lines inferred from Polar plasma wave data, *J. Geophys. Res.*, **106**(A4), 6195-6201, doi:10.1029/2000JA000068.

Greenwald, R.A., Baker, K.B., Dudeney, J.R., Pinnock, M., Jones, T.B., Thomas, E.C., Villain, J.R., Cerisier. J.C., Senior, C., Hanuise, C., Hunsucker, R.D., Sofko, G., Koehler, J., Nielsen, E., Pellinen, R., Walker, A.D.M., Sato, N., and Yamagishi, H. (1995) A Global View of the Dynamics of High-Latitude Convection, *Space Sci. Rev.*, **71**, 761-796.

Hori, T., Shinbori, A., Nishitani, N., Kikuchi, T., Fujita, S., Nagatsuma, T., Troshichev, O., Yumoto, K., Moiseyev, A., and Seki, K. (2012) Evolution of negative SI-induced ionospheric flows observed by SuperDARN King Salmon HF radar, *J. Geophys. Res.*, **117**, A12223. doi:10.1029/2012JA018093.,

Kale, Z.C., Mann, I.R., Waters, C.L., Vellante, M., Zhang, T.L., and Honary, F. (2009) Plasmaspheric dynamics resultin from the Hallowe'en 2003 geomagnetic storms, *J. Geophys. Res.*, **114**, A08204, doi:10.1029/2009JA014194.

Kawano, H., Yumoto, K., Pilipenko, V.A., Tanaka, Y.M., Takasaki, S., Iizima, M., and Seto, M. (2002) Using two ground stations to identify magnetospheric field line eigenfrequency as a continuous function of ground latitude, *J. Geophys. Res.*, **107**, doi:10.1029/2001JA000274.

Kivelson, M.G. and Southwood, D.J. (1985) Resonant ULF waves: A new interpretation, *Geophys. Res. Lett.*, **12**, 49-52, doi:10.1029/GL012i001p00049.

Kivelson, M.G. and Southwood, D.J. (1986), Coupling of global magnetospheric MHD eigenmodes to Field line resonances, *J. Geophys. Res.*, **91**, 4345-4351, doi:10.1029/JA091iA04p04345.

Kokubun, S. (2013) ULF waves in the outer magnetosphere: Geotail observation 1 transverse waves, *Earth Planets Space*, **65**, 411-433.

Liu, J.J., Hu, H.Q., Han, D.S., Liu, Y.H., Zhang, Q.H., and Yukimatu, A.S. (2013) Optical and SuperDARN radar observations of duskside shock aurora over Zhongshan Station. *Adv. Polar Sci.*, **24**, 60-68, doi: 10.3724/SP.J.1085.2013.00060.

Liu, W, Sarris, T.E., Li, X, Elkington, S.R., Ergun, R., Angelopoulos, V., Bonnell, J., and Glassmeier, K.H. (2009) Electric and magnetic field observations of Pc4 and Pc5 pulsations in the inner magnetosphere: A statistical

study, *J. Geophys. Res.*, **114**, A12206. doi:10.1029/2009JA014243.

Lockwood, M., Sandholt, P.E., Cowley, S.W.H., and Oguti, T. (1989) Interplanetary magnetic field control of dayside auroral activity and the transfer of momentum across the dayside magnetopause. *Planet. Space Sci.*, **37**(11), 1347-1365. doi:10.1016/0032-0633(89)90106-2.

Nedie, A.Z., Rankin, R., and Fenrich, F.R. (2012) SuperDARN observations of the driver wave associated with FLRs, *J. Geophys. Res.*, **117**(A6), CiteID A06232.

Nishitani, N., Ogawa, T., Otsuka, Y., Hosokawa, K., and Hori, T. (2011) Propagation of large amplitude ionospheric disturbances with velocity dispersion observed by the SuperDARN Hokkaido radar after the 2011 off the Pacific coast of Tohoku earthquake, *Earth Planets Space*, **63**, 891-896.

Obana, Y., Menk, F.W., Sciffer, M.D., and Waters, C.L. (2008) Quarter-wave modes of standing Alfve´n waves detected by cross-phase analysis, *J. Geophys. Res.*, **113**, A08203. doi:10.1029/2007JA012917.

Obana, Y., Waters, C.L., Sciffer, M.D., Menk, F.W., Lysak, R.L., Shiokawa, K., Hurst, A.W., and Petersen, T. (2015), Resonance structure and mode transition of quarter-wave ULF pulsations around the dawn terminator, *J. Geophys. Res.*, **120**, doi:10.1002/2015JA021096.

Pilipenko V.A. and Fedorov, E.N. (1994) Magnetotelluric sounding of the crust and hydrodynamic monitoring of the magnetosphere with the use of ULF waves, In M.J.Engebretson, K.Takahashi, and M.Scholer(ed) Solar Wind Sources of Magnetospheric Ultra-Low-Frequency Waves, *Geophys. Monogr. Ser.*, **81**, AGU, Washington, DC, p 283-292.

Ponomarenko, P.V., Menk, F.W., and Waters, C.L. (2003) Visualization of ULF waves in SuperDARN data, *Geophys. Res. Lett.*, **30**, 1926-1929. doi:10.1029/2003GL017757.

Ponomarenko, P.V., Menk, F.W., Waters, C.L., and Sciffer, M. (2005) Pc3-4 ULF waves observed by the SuperDARN TIGER radar, *Ann. Geophys.*, **23**, 1271-1280. doi:10.5194/angeo-23-1271-2005.

Picone, J.M., Hedin, A.E., Drob, D.P., and Aikin, A.C. (2002) NRLMSISE-00 empirical model of the atmosphere: Statistical comparisons and scientific issues, *J. Geophys. Res.*, **107**(A12), 1468, doi:10.1029/2002JA009430.

Rae, I.J., Donovan, E.F., Mann. I.R., Fenrich, F.R., Watt, C.E.J., Milling, D.K., Lester, M., Lavraud, B., Wild, J.A., Singer, H.J., Rème, H., and Balogh, A. (2005) Evolution and characteristics of global Pc5 ULF waves during a high solar wind speed interval, *J. Geophys. Res.*, **110**, A12211, doi:10.1029/2005JA011007.

Ribeiro A.J., Ruohoniemi, J.M., Baker, J.B.H., Clausen, L.B.N., de Larquier, S., and Greenwald, R.A. (2011) A new approach for identifying ionospheric backscatter in midlatitude SuperDARN HF radar observations, *Radio Sci.*, **46**, RS4011. doi:10.1029/2011RS004676.

Sakaguchi, K., Nagatsuma, T., Ogawa, T., Obara, T., and Troshichev, O.A. (2012) Ionospheric Pc5 plasma oscillations observed by the King Salmon HF radar and their comparison with geomagnetic pulsations on the ground and in geostationary orbit, *J. Geophys. Res.*, **117**, A03218, doi:10.1029/2011JA016923.

Samson, J.C., Jacobs, J.A., and Rostoker, G. (1971) Latitude-dependent characteristics of long-period geomagnetic micropulsations, *J. Geophys. Res.*, **76**, 3675-3683. doi:10.1029/JA076i016p0367.

Singer, H.J. and Kivelson, M.G. (1979) The latitudinal structure of Pc 5 waves in space: Magnetic and electric field observations, *J. Geophys. Res.*, **84**, 7213-7222. doi:10.1029/JA084iA12p07213.

Singer, H.J., Southwood, D.J., Walker, R.J., and Kivelson, M.G. (1981) Alfvén wave resonances in a realistic magnetospheric magnetic field geometry, *J. Geophys. Res.*, **86**(A6), 4589-4596, doi:10.1029/JA086iA06p04589.

Southwood, D.J. (1974) Some features of field line resonances in the magnetosphere, *Planet. Space Sci.*, **22**, 483-491.

Takahashi, K., R. E. Denton, R. R. Anderson, and W. J. Hughes (2004) Frequencies of standing Alfvén wave harmonics and their implication for plasma mass distribution along geomagnetic field lines: Statistical analysis of CRRES data, *J. Geophys. Res.*, **109**, A08202, doi:10.1029/2003JA010345.

Takahashi, K., Bonnell, J., Glassmeier, K.-H., Angelopoulos, V., Singer, H.J., Chi, P.J., Denton, R.E., Nishimura, Y., Lee, D.-H., Nosé, M., and Liu, W. (2010) Multipoint observation of fast mode waves trapped in the dayside plasmasphere, *J. Geophys. Res.*, **115**, A12247, doi:10.1029/2010JA015956.

Takasaki, S., Kawano, H., Tanaka, Y., Yoshikawa, A., Seto, M., Iizima, M., Obana, Y., Sato, N., and Yumoto, K. (2006) A significant mass density increase during a large magnetic storm in October 2003 obtained by ground-based ULF observations at L ~ 1.4, *Earth Planets Space*, **58**, 617-622.

Tamao, T. (1965) Transmission and coupling resonance of hydromagnetic disturbances in the non-uniform Earth's magnetosphere, *Sci. Rep. Tohoku Univ. Ser.* **5***, Geophys.* **17**, 43-72.

Tsyganenko, N.A. and Sitnov, M.I. (2005) Modeling the dynamics of the inner magnetosphere during strong geomagnetic storms, *J. Geophys. Res.*, **110**, A03208, doi:10.1029/2004JA010798.